

## Conduction at a Ferroelectric Interface

M. S. J. Marshall,<sup>1,2</sup> A. Malashevich,<sup>1,2</sup> A. S. Disa,<sup>1,2</sup> M. G. Han,<sup>3</sup> H. Chen,<sup>1,2</sup> Y. Zhu,<sup>3</sup> S. Ismail-Beigi,<sup>1,2</sup> F. J. Walker,<sup>1,2</sup> C. H. Ahn\*<sup>1,2,4</sup>

1. Center for Research on Interface Structures and Phenomena (CRISP), Yale University, New Haven, CT 06520, USA

2. Dept. of Applied Physics, Yale University, New Haven, CT 06520, USA

3. Dept. of Condensed Matter Physics and Materials Science, Brookhaven National Laboratory, Upton, NY 11973, USA

4. Dept. of Mechanical Engineering and Materials Science, Yale University, New Haven, CT 06520, USA

\*charles.ahn@yale.edu

Typical logic elements utilizing the field effect rely on the change in carrier concentration due to the field in the channel region of the device. Ferroelectric field effect devices provide a non-volatile version of this effect due to the stable polarization order parameter in the ferroelectric. In this work, we describe an oxide/oxide ferroelectric heterostructure device based on (001)-oriented  $\text{PbZr}_{0.2}\text{Ti}_{0.8}\text{O}_3$  (PZT)- $\text{LaNiO}_3$  where the dominant change in conductivity is a result of a significant mobility change in the interfacial channel region. The effect is confined to a few atomic layers at the interface, and is reversible by switching the ferroelectric polarization. More interestingly, in one polarization state the field effect induces a 1.7 eV shift of the interfacial bands to create a new conducting channel in the interfacial PbO layer of the ferroelectric.

Electronic devices based on the ferroelectric field effect are designed with two functional components, a ferroelectric gate and a conducting channel. The device operates via large changes in carrier density in the conducting channel, which is controlled by the ferroelectric polarization [1]. Here we describe a device where a single atomic layer in the ferroelectric itself serves as the conducting channel. Generally, ferroelectricity and metallicity are incompatible in the bulk because conduction electrons screen the bulk polarization [2], but it has been predicted that metallic states form at ferroelectric surfaces due to the large electric fields present at surfaces where the polarization terminates [3-6]. Here, we describe a device heterostructure where this mechanism operates at a  $\text{PbZr}_{0.2}\text{Ti}_{0.8}\text{O}_3$  (PZT)- $\text{LaNiO}_3$  interface. When the polarization direction points away from the interface, the normally fully occupied PbO bands of the interfacial PZT cross the Fermi level to form a conducting channel. In this approach, the

properties of the channel material,  $\text{LaNiO}_3$ , are critical for the formation of the metallic state in the ferroelectric. In order to induce a ferroelectric interface that becomes metallic, the material adjacent to the ferroelectric must be sufficiently conductive to provide carriers that screen the polarization, but also sufficiently resistive to avoid shorting out conductivity in the ferroelectric. While  $\text{LaNiO}_3$  is fully metallic in the bulk, ultra-thin films of  $\text{LaNiO}_3$  can have low conductivity due to structural distortions [7], spin scattering, and scattering from boundaries [8].

Because of the focus on interfacial metallic states, their contribution to the electronic transport will be most pronounced for channels of ultra-thin films with atomically abrupt interfaces. To realize these structures, oxygen-plasma assisted molecular beam epitaxy is used to grow  $\text{LaNiO}_3$  films on  $\text{AlO}_2$ -terminated (001)-oriented  $\text{LaAlO}_3$  substrates, which are pre-patterned with Hall bar devices. The substrate temperature is  $590\text{ }^\circ\text{C}$  during deposition at an oxygen partial pressure of  $\sim 5.4 \times 10^{-6}$  Torr. Oscillations of the reflection high-energy electron diffraction (RHEED) specular spot intensity are monitored *in situ* to determine the film thickness. A 150 - 200 nm thick layer of  $\text{PbZr}_{0.2}\text{Ti}_{0.8}\text{O}_3$  (PZT) is grown using off-axis RF magnetron sputtering at  $520\text{ }^\circ\text{C}$ , in 225 mTorr of Ar :  $\text{O}_2$  (1 : 3 ratio). The PZT/ $\text{LaNiO}_3$  structures are cooled to room temperature in the process gases, to avoid the formation of vacancies that may adversely affect the ferroelectric switching [9, 10]. TEM sample preparation is performed using a focused-ion beam (FIB) lift-out technique. After FIB milling, low energy (0.9 keV) Ar ion milling with a Nanomill (E. A. Fischione Instruments, Inc.) is used to remove FIB-induced sample damage. A JEOL ARM 200CF microscope equipped with a cold field-emission electron gun and double spherical-aberration correctors (CEOS GmbH) is used for high-angle annular-dark-field (HAADF) scanning transmission electron microscopy (STEM) imaging. The collection angles are in the range of 68 to 280 mead. The first-principles

calculations are based on density functional theory (DFT) within the periodic supercell plane-wave pseudopotential approach, as implemented in the Quantum ESPRESSO software package [11]. The LaNiO<sub>3</sub>-PZT interface is modeled as a slab containing four  $c(2 \times 2)$  unit cells of LaNiO<sub>3</sub> in contact with 3.5 unit cells of PbTiO<sub>3</sub>. To simulate the effect of the LaAlO<sub>3</sub> substrate, the in-plane lattice parameter of the slab is strained to the value corresponding to bulk LaAlO<sub>3</sub>, computed within the same theoretical framework. Vanderbilt ultrasoft pseudopotentials are employed to describe atoms [12]. We have chosen to use the local-density approximation (LDA) with the Perdew-Zunger parameterization [13] to describe the exchange-correlation potential, since Gou *et al.* found that LDA was more appropriate to study LaNiO<sub>3</sub> compared to other functionals [14]. We use a 35 Ry plane-wave energy cut-off for the wavefunctions and a 280 Ry cut-off for the electron density. Each slab is separated from its periodic image by  $\sim 10$  Å. The Brillouin zone is sampled by a regular  $4 \times 4 \times 1$  mesh of  $k$  points. To simulate the accumulation and depletion states, the polarization state of PbTiO<sub>3</sub> is set by fixing the atomic positions of one-unit-thick layer of PbTiO<sub>3</sub> furthest from the interface to corresponding theoretical values of polarized bulk PbTiO<sub>3</sub> strained to LaAlO<sub>3</sub>. Following the structural relaxation, we verify that the entire PbTiO<sub>3</sub> is in the desired polar state. To reduce the artificial polarization effects from the surface charges, the terminal PbO layer facing the vacuum is covered by two layers of Pt, which also serve as the electron reservoir (electrode) for the system. To check that there is no spurious effect from the electric field in the vacuum region, we applied the dipole correction technique [15], which we found to have negligible impact on the crystal structure and the electronic structure of the interface (Fig. S5). Structural relaxation of the two slabs modeling the accumulation and depletion states of the interface is performed until all Cartesian components of the forces on all atoms are 30 meV/Å in magnitude. In order to project the electronic band

structure onto the various structural components, we compute maximally localized Wannier functions [16, 17] using the Wannier90 software package [18]. The spatial locality of the Wannier functions then allows us to disentangle the bands of interest (with Ni or Pb character) from the Pt bands crossing the Fermi level, as the latter are not related to or of interest for the electronic structure of the  $\text{PbTiO}_3/\text{LaNiO}_3$  interface.

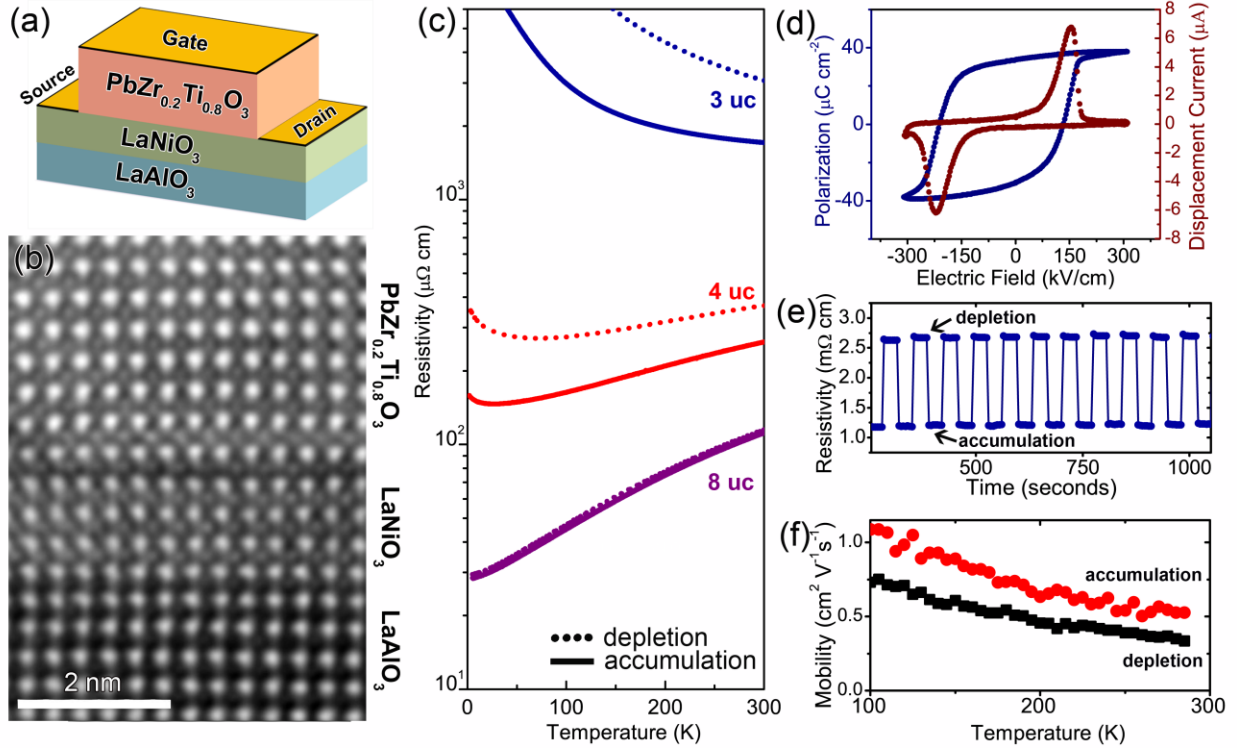


FIG. 1. Resistivity and switching behavior of  $\text{PbZr}_{0.2}\text{Ti}_{0.8}\text{O}_3/\text{LaNiO}_3$  devices. (a) Schematic of the PZT/ $\text{LaNiO}_3$  devices, shown with gold electrodes. (b) Cross-sectional transmission electron micrograph of a PZT/4 uc  $\text{LaNiO}_3$  device. (c) Resistivity versus temperature for PZT/ $\text{LaNiO}_3$  devices with  $\text{LaNiO}_3$  thicknesses of 3 uc, 4 uc and 8 uc (solid and dotted lines correspond to accumulation and depletion of holes, respectively). (d) The polarization-electric field (P-E) loop obtained from a structure of 150 nm PZT/ 3 uc  $\text{LaNiO}_3$ . The remnant polarization is  $\approx 30 \mu\text{C}/\text{cm}^2$ . In (e) the room-temperature resistivity of a 3 uc  $\text{LaNiO}_3$  device is shown as a function

of time as the system is switched from the low resistance state (accumulation of holes) to the high resistance state (depletion of holes). (f) Polarization-dependent carrier mobility determined from Hall measurements for a PZT/4 uc LaNiO<sub>3</sub> device.

A schematic of the device structure is shown in Fig. 1(a). As seen from the transmission electron micrograph in Fig. 1(b), these device structures display atomically sharp interfaces. The PZT layer exhibits a well defined hysteresis in the polarization versus electric field (P-E) loop [Fig. 1(d)], measured using a positive-up negative-down (PUND) method [19]. Hall measurements indicate that transport in LaNiO<sub>3</sub> is hole-like, in agreement with previously reported measurements [7, 8]. The ferroelectric polarization thus depletes hole carriers from the PZT/LaNiO<sub>3</sub> interface when the polarization direction points towards the nickelate (depletion state), and accumulates hole carriers at the interface when the direction of polarization points away from the nickelate layer (accumulation state). This polarization couples to the electrical properties of the nickelates, as shown in the resistivity versus temperature plots for the PZT/LaNiO<sub>3</sub> devices [Fig. 1(c)], for which the thicknesses of the LaNiO<sub>3</sub> are 3 uc, 4 uc and 8 uc. The resistivity of the 8 uc LaNiO<sub>3</sub> film is bulk-like and metallic down to 2 K for both polarization states of PZT. The resistivity of the 4 uc thick film shows a distinct change in behavior at low temperatures. In the depletion state, the 4 uc thick film has a metal-insulator transition at  $\approx 75$  K. In contrast, the accumulation state of the 4 uc thick film is metallic down to  $\approx 20$  K. The 3 uc thick LaNiO<sub>3</sub> film is insulating at all temperatures, exhibiting a factor of two change in room temperature resistivity when switched from accumulation to depletion. Applying a train of 100 ms long voltage pulses at room temperature to switch the polarization of the ferroelectric reveals reversible and non-volatile switching of the LaNiO<sub>3</sub> resistivity [Fig. 1(e)].

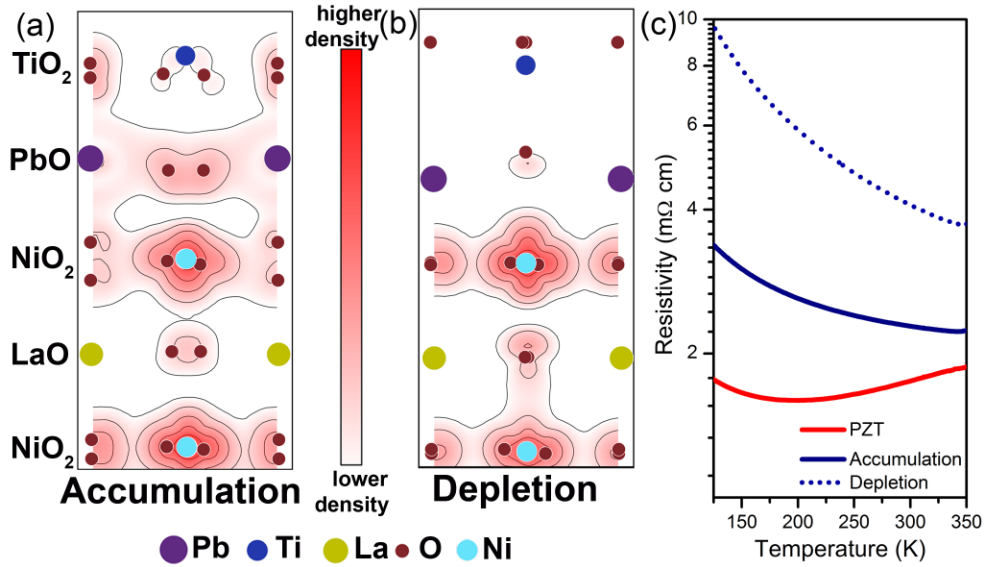


FIG. 2. Electronic structure of PTO/4 uc LaNiO<sub>3</sub> strained to the theoretical in-plane lattice constant of LaAlO<sub>3</sub>. A 2D projection of the local density of electronic states derived from first-principles calculations integrated within  $\pm k_B T$  eV of the Fermi level ( $T = 300$  K) at the interface of PbTiO<sub>3</sub> and LaNiO<sub>3</sub> for (a) the accumulation state and (b) the depletion state. The red contours indicate a higher density of states, and the white areas indicate a lower density of states. (c) Temperature dependent resistivity measurements for devices with 3 uc-thick LaNiO<sub>3</sub> in the accumulation (solid blue) and depletion states (dashed blue). The resistivity, normalized to 1 uc of interfacial PZT, is also shown (red). A zoomed-out version is shown in Fig. S1.

To elucidate the origin of the polarization-dependent changes in resistivity, we measure the carrier concentration of the channel for both polarization directions on a device with a 4 uc LaNiO<sub>3</sub> channel. Hall measurements show that conduction is dominated by majority hole carriers, with a carrier concentration of  $\approx 5 \times 10^{22} \text{ cm}^{-3}$  at 285 K. This value corresponds to 3 holes/uc, in agreement with band theory and measurements of thin films of LaNiO<sub>3</sub> [20-23].

From the value of the remnant polarization of the PZT ( $25 \mu\text{C}/\text{cm}^2$ ), we expect the change in carrier concentration for a 4 uc thick  $\text{LaNiO}_3$  device to be  $\approx 2\%$  if we assume that most charge is screened within one interfacial unit cell of the nickelate. This value of 2% is much smaller than the measured change in conductivity of 30% for a 4 uc thick  $\text{LaNiO}_3$  device (Fig. 1(c)), and thus one finds that the change in mobility is about 30%, as shown in Fig. 1(f). A modulation of mobility is unexpected and distinct from the modulation of conductivity for semiconductor devices, which rely on changes in the carrier concentration to modify the conductivity [9, 24-26]. This result is also distinct from those obtained using electrolytically gated  $\text{NdNiO}_3$  thin films, where the mobility is unchanged when a large polarization is applied[21]. Hence, we expect that the details of the physical and electronic structure at the interface play a key role, where changing the PZT polarization distorts the interfacial structure, in addition to changing the carrier concentration [27].

To predict changes in the physical and electronic structure, we turn to first-principles calculations and compute the local electron density for the ground state structures of each polarization state [Figs. 2(a) and 2(b)]. In the accumulation state, there is significant density in the PbO layer of the  $\text{PbTiO}_3$  closest to the interface, which is notably absent in the depletion state. We understand the presence of states at the Fermi level in the PbO layer by examining the band structures shown in Fig. 3(a) (accumulation) and Fig. 3(b) (depletion). For the accumulation state [Fig. 3(a)], we observe bands with strong Pb character at the Fermi level, in which Pb 6s states hybridize with O 2p states. In the depletion state [Fig. 3(b)], these Pb-related states are absent close to the Fermi level, showing that the bands crossing the Fermi level have no Pb character and arise exclusively from Ni and O. Similarly, the layer-resolved LDOS is plotted in accumulation [Fig. 3(c)] and depletion [Fig. 3(d)], where it is evident that significant

LDOS are present in the interfacial layer of  $\text{PbTiO}_3$  at the interface in accumulation, but not in depletion. The origin of PbO character in bands that cross the Fermi level is two-fold. First, the electric field due to the ferroelectric field effect shifts the PbO bands upwards to cross the Fermi level in the accumulation state by about 1.7 V, as predicted to occur at vacuum- $\text{PbTiO}_3$  surfaces for the same polarization direction<sup>18</sup>. The magnitude of the shift is also consistent with the magnitude of the ferroelectric polarization. Second, the change in apical oxygen bond length in the top-most nickelate layer facilitates hybridization between Ni and Pb. As the apical oxygen moves further away from the  $\text{NiO}_2$  layer in the depletion state, hybridization between Pb states with those of Ni and O is suppressed. Density functional theory predicts the appearance of an additional channel for conduction in the PbO layer of the ferroelectric. We estimate an upper bound for the resistivity of this layer by taking the difference in conductance in accumulation and depletion [Fig. 2(c)]. Strikingly, even though the film as a whole has insulating character, the additional conductivity of the channel has a metallic temperature dependence. The role of  $\text{NiO}_6$  and  $\text{TiO}_6$  octahedral rotations may also be tested by calculating the layer-resolved LDOS using a  $1 \times 1$  supercell, which suppresses all octahedral tilts and rotations, as shown in Fig. S2. This indicates that the appearance of a conductive PbO state at the interface in the accumulation state is not directly related to octahedral rotations.

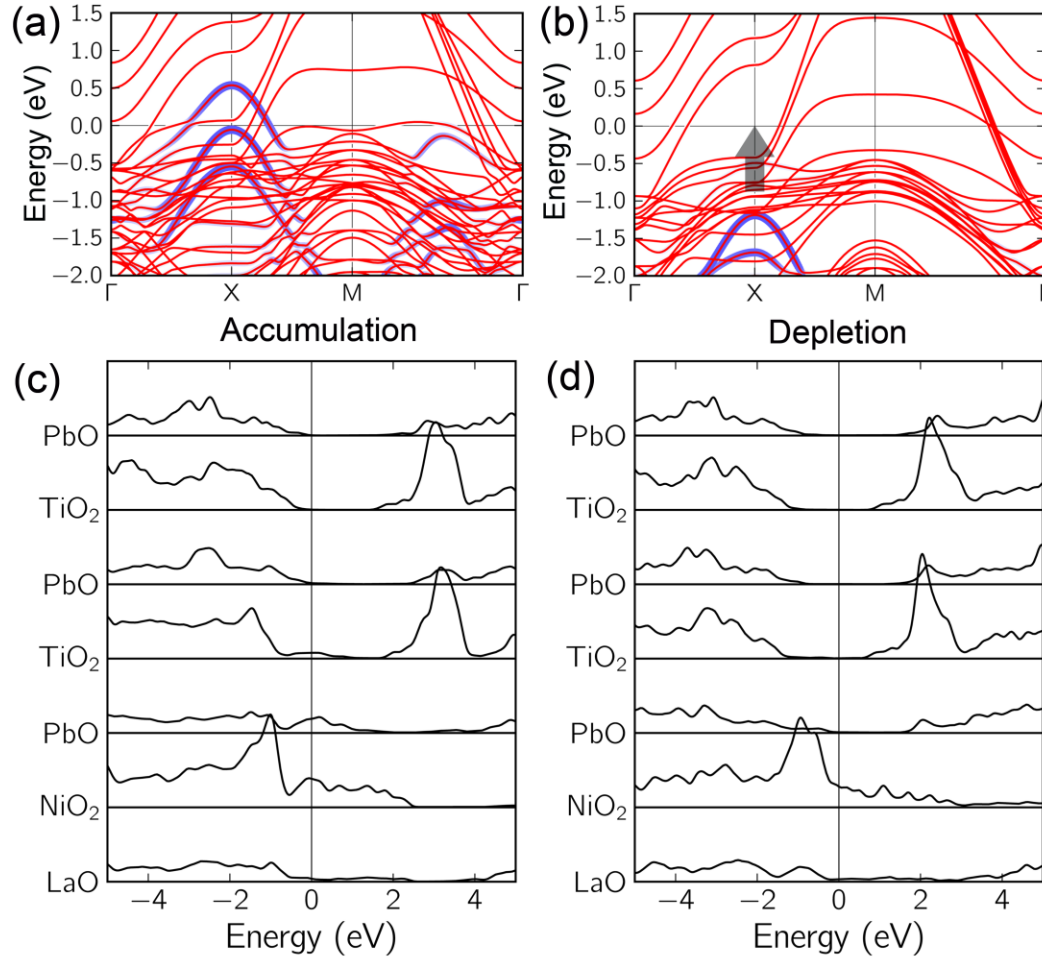


FIG. 3. Band structure of PTO/  $\text{LaNiO}_3$  strained to the theoretical in-plane lattice constant of  $\text{LaAlO}_3$ . Band structure for (a) accumulation and (b) depletion, where the zero of energy is the Fermi level in each case and a  $(1 \times 1)$  interfacial unit cell is employed. Red-colored bands correspond to dominant  $\text{LaNiO}_3$  character, while blue-colored bands indicate strong contributions from the interfacial  $\text{PbO}$  layer. The top of the  $\text{PbO}$ -dominated bands shift from about  $-1.2$  eV in depletion to approximately  $0.5$  eV in accumulation. (c) The layer-resolved LDOS at the interface for accumulation, and (d) depletion. The  $\text{PbTiO}_3$  is insulating in depletion, and is insulating in accumulation away from the interface, which has LDOS at the Fermi level.

While these theoretical calculations are theoretically self-consistent, they also explain the experimentally measured changes in conductivity. To test the robustness of the calculations, we calculated a structure in which the  $\text{LaNiO}_3$  is 3 uc thick (Fig. S4), performed an LDA+U calculation where  $U = 3$  eV on the Ni d site (Fig. S3), and applied a dipole correction to ensure zero electric field in the vacuum region (Fig. S5) [28]. All of these calculations are in agreement with the results presented in Fig. 3, reinforcing the robustness of the DFT results. These results show that the ferroelectric polarization induces a robust metallic state in the ferroelectric at the interface. This state forms by electrostatically shifting the valence bands of PZT upward to cross the Fermi level of the  $\text{LaNiO}_3$  channel. In addition, the ferroelectric polarization strongly modifies the bond lengths involving Ni, O, and Pb across the interface, which in turn hybridizes the Ni, O, and Pb states to facilitate charge redistribution into the PZT layer. What results is a change in carrier mobility, as carriers redistribute into the higher mobility channel in PZT. The mobility of the PbO layer may be higher than that of  $\text{LaNiO}_3$  due to a smaller effective mass [29] or due to reduced scattering. In particular,  $\text{PbTiO}_3$  is likely less susceptible to hole carrier scattering with spins, which is expected to contribute to the resistivity of  $\text{LaNiO}_3$  due to the  $d^7$  electron configuration of the Ni sites<sub>[8]</sub>. Such metallic states in ferroelectrics have been recently predicted using first principles density functional theory [6, 30, 31]. These works focus on conduction at surfaces, rather than at interfaces [6]. Such surface states on ferroelectrics can be challenging to realize experimentally due to surface reconstructions and screening by adsorbates. While interface structure can influence the polarization [32, 33], the ferroelectric does not undergo such a reconstruction at an interface [34, 35].

The mechanism for interfacial conductivity in a ferroelectric is general and raises possibilities for engineering buried interfaces. For instance, the layer of PbO at the interface can be replaced with

a single atomic layer of another material with enhanced conductive, ferroelectric, or magnetic properties. Moreover, the use of a ferroelectric interface enables dynamic reversible control via switching of the polarization. This effect may be useful in realizing novel ferroelectric field effect devices that function in a mechanistically different way than existing technology.

### **Acknowledgements:**

Work at Yale is supported by the Office of Naval Research, NSF DMR 1119826 (CRISP), and the DARPA OLE Program under an Army Research Office Grant No. W911NF-10-1-0206.

Work at the Center for Functional Nanomaterials, Brookhaven National Laboratory is supported by the U.S. Department of Energy, Office of Basic Energy Sciences Division of Materials Science and Engineering, under Contract number DE-AC02-98CH10886. The authors thank Eric Altman and Divine Kumah for helpful discussions.

### **References:**

- [1] K. M. Rabe, C. H. Ahn, and J.-M. Triscone, *Physics of Ferroelectrics: a Modern Perspective* (Springer, 2007), Vol. 105.
- [2] P. W. Anderson, and E. I. Blount, Symmetry Considerations on Martensitic Transformations: "Ferroelectric" Metals?, *Phys. Rev. Lett.* **14** 217 (1965).
- [3] T. Kolodiaznyi, M. Tachibana, H. Kawaji, J. Hwang, and E. Takayama-Muromachi, Persistence of Ferroelectricity in BaTiO<sub>3</sub> through the Insulator-Metal Transition, *Phys. Rev. Lett.* **104** 147602 (2010).
- [4] Y. Wang, X. Liu, J. D. Burton, S. S. Jaswal, and E. Y. Tsymlal, Ferroelectric Instability Under Screened Coulomb Interactions, *Phys. Rev. Lett.* **109** 247601 (2012).
- [5] Y. Shi, Y. Guo, X. Wang, A. J. Princep, D. Khalyavin, P. Manuel, Y. Michiue, A. Sato, K. Tsuda, and S. Yu, A ferroelectric-like structural transition in a metal, *Nat. Mater.* **12** 1024 (2013).
- [6] J. He, G. Stephenson, and S. Nakhmanson, Electronic surface compensation of polarization in PbTiO<sub>3</sub> films, *J. Appl. Phys.* **112** 054112 (2012).
- [7] D. P. Kumah, A. Disa, J. Ngai, H. Chen, J. Reiner, S. Ismail-Beigi, F. Walker, and C. Ahn, Tuning the Structure of Nickelates to Achieve Two-dimensional Electron Conduction, *Adv. Mater.* (2014).
- [8] R. Scherwitzl, S. Gariglio, M. Gabay, P. Zubko, M. Gibert, and J.-M. Triscone, Metal-Insulator Transition in Ultrathin LaNiO<sub>3</sub> Films, *Phys. Rev. Lett.* **106** 246403 (2011).
- [9] C. A. F. Vaz, Y. Segal, J. Hoffman, F. J. Walker, and C. H. Ahn, Growth and characterization of PZT/LSMO multiferroic heterostructures, *J. Vac. Sci. Tech. B* **28** C5A6 (2010).
- [10] C. T. Nelson *et al.*, Domain dynamics during ferroelectric switching, *Science* **334** 968 (2011).
- [11] P. Giannozzi, S. Baroni, N. Bonini, M. Calandra, R. Car, C. Cavazzoni, D. Ceresoli, G. L. Chiarotti, M. Cococcioni, and I. Dabo, QUANTUM ESPRESSO: a modular and open-source software project for quantum simulations of materials, *J. Phys.: Cond. Matt.* **21** 395502 (2009).

- [12] D. Vanderbilt, Soft self-consistent pseudopotentials in a generalized eigenvalue formalism, *Phys. Rev. B* **41** 7892(R) (1990).
- [13] J. P. Perdew, and A. Zunger, Self-interaction correction to density-functional approximations for many-electron systems, *Phys. Rev. B* **23** 5048 (1981).
- [14] G. Gou, I. Grinberg, A. M. Rappe, and J. M. Rondinelli, Lattice normal modes and electronic properties of the correlated metal  $\text{LaNiO}_3$ , *Phys. Rev. B* **84** 144101 (2011).
- [15] L. Bengtsson, Dipole correction for surface supercell calculations, *Phys. Rev. B* **59** 12301 (1999).
- [16] N. Marzari, and D. Vanderbilt, Maximally localized generalized Wannier functions for composite energy bands, *Phys. Rev. B* **56** 12847 (1997).
- [17] I. Souza, N. Marzari, and D. Vanderbilt, Maximally localized Wannier functions for entangled energy bands, *Phys. Rev. B* **65** 035109 (2001).
- [18] A. A. Mostofi, J. R. Yates, Y.-S. Lee, I. Souza, D. Vanderbilt, and N. Marzari, wannier90: A tool for obtaining maximally-localised Wannier functions, *Comp. Phys. Comm.* **178** 685 (2008).
- [19] K. M. Rabe, M. Dawber, C. Lichtensteiger, C. H. Ahn, and J.-M. Triscone, in *Physics of Ferroelectrics* (Springer, 2007), pp. 1.
- [20] R. Scherwitzl, P. Zubko, C. Lichtensteiger, and J.-M. Triscone, Electric-field tuning of the metal-insulator transition in ultrathin films of  $\text{LaNiO}_3$ , *Appl. Phys. Lett.* **95** 222114 (2009).
- [21] R. Scherwitzl, P. Zubko, G. Lezama, S. Ono, A. Morpurgo, G. Catalan, and J.-M. Triscone, Electric-Field Control of the Metal-Insulator Transition in Ultrathin  $\text{NdNiO}_3$  films, *Adv. Mater.* **22** 5517 (2010).
- [22] J. Son, P. Moetakef, J. M. LeBeau, D. Ouellette, L. Balents, S. J. Allen, and S. Stemmer, Low-dimensional Mott material: Transport in ultrathin epitaxial  $\text{LaNiO}_3$  films, *Appl. Phys. Lett.* **96** 062114 (2010).
- [23] N. Gayathri, A. K. Raychaudhuri, X. Q. Xu, J. L. Peng, and R. L. Greene, Electronic conduction in: the dependence on the oxygen stoichiometry, *J. Phys.: Cond. Matt.* **10** 1323 (1998).
- [24] C. H. Ahn, J.-M. Triscone, and J. Mannhart, Electric field effect in correlated oxide systems, *Nature* **424** 1015 (2003).
- [25] C. A. F. Vaz, J. Hoffman, Y. Segal, J. W. Reiner, R. D. Grober, Z. Zhang, C. H. Ahn, and F. J. Walker, Origin of the Magnetoelectric Coupling Effect in  $\text{PbZr}_{0.2}\text{Ti}_{0.8}\text{O}_3/\text{La}_{0.8}\text{Sr}_{0.2}\text{MnO}_3$  Multiferroic Heterostructures, *Phys. Rev. Lett.* **104** 127202 (2010).
- [26] S. Mathews, R. Ramesh, T. Venkatesan, and J. Benedetto, Ferroelectric field effect transistor based on epitaxial perovskite heterostructures, *Science* **276** 238 (1997).
- [27] H. Chen, D. P. Kumah, A. S. Disa, F. J. Walker, C. H. Ahn, and S. Ismail-Beigi, Modifying the Electronic Orbitals of Nickelate Heterostructures via Structural Distortions, *Phys. Rev. Lett.* **110** 186402 (2013).
- [28] See Supplemental Material at [URL will be inserted by publisher] for supporting density of states plots.
- [29] G. Hautier, A. Miglio, G. Ceder, G.-M. Rignanese, and X. Gonze, Identification and design principles of low hole effective mass *p*-type transparent conducting oxides, *Nat. Commun.* **4**(2013).
- [30] M. Stengel, P. Aguado-Puente, N. A. Spaldin, and J. Junquera, Band alignment at metal/ferroelectric interfaces: Insights and artifacts from first principles, *Phys. Rev. B* **83** 235112 (2011).
- [31] Y. Watanabe, M. Okano, and A. Masuda, Surface conduction on insulating  $\text{BaTiO}_3$  crystal suggesting an intrinsic surface electron layer, *Phys. Rev. Lett.* **86** 332 (2001).
- [32] H. N. Lee, H. M. Christen, M. F. Chisholm, C. M. Rouleau, and D. H. Lowndes, Strong polarization enhancement in asymmetric three-component ferroelectric superlattices, *Nature* **433** 395 (2005).
- [33] M. Stengel, D. Vanderbilt, and N. A. Spaldin, Enhancement of ferroelectricity at metal-oxide interfaces, *Nat. Mater.* **8** 392 (2009).
- [34] A. M. Kolpak, D. Li, R. Shao, A. M. Rappe, and D. A. Bonnell, Evolution of the structure and thermodynamic stability of the  $\text{BaTiO}_3$  (001) surface, *Phys. Rev. Lett.* **101** 036102 (2008).

[35] C. Noguera, Polar oxide surfaces, *J. Phys.: Cond. Matt.* **12** R367 (2000).